The European Physical Journal

volume 37 · number 10 · october · 2014

EPJ E

FOUNDED BY PIERRE-GILLES DE GENNES

Recognized by European Physical Society

Soft Matter and Biological Physics

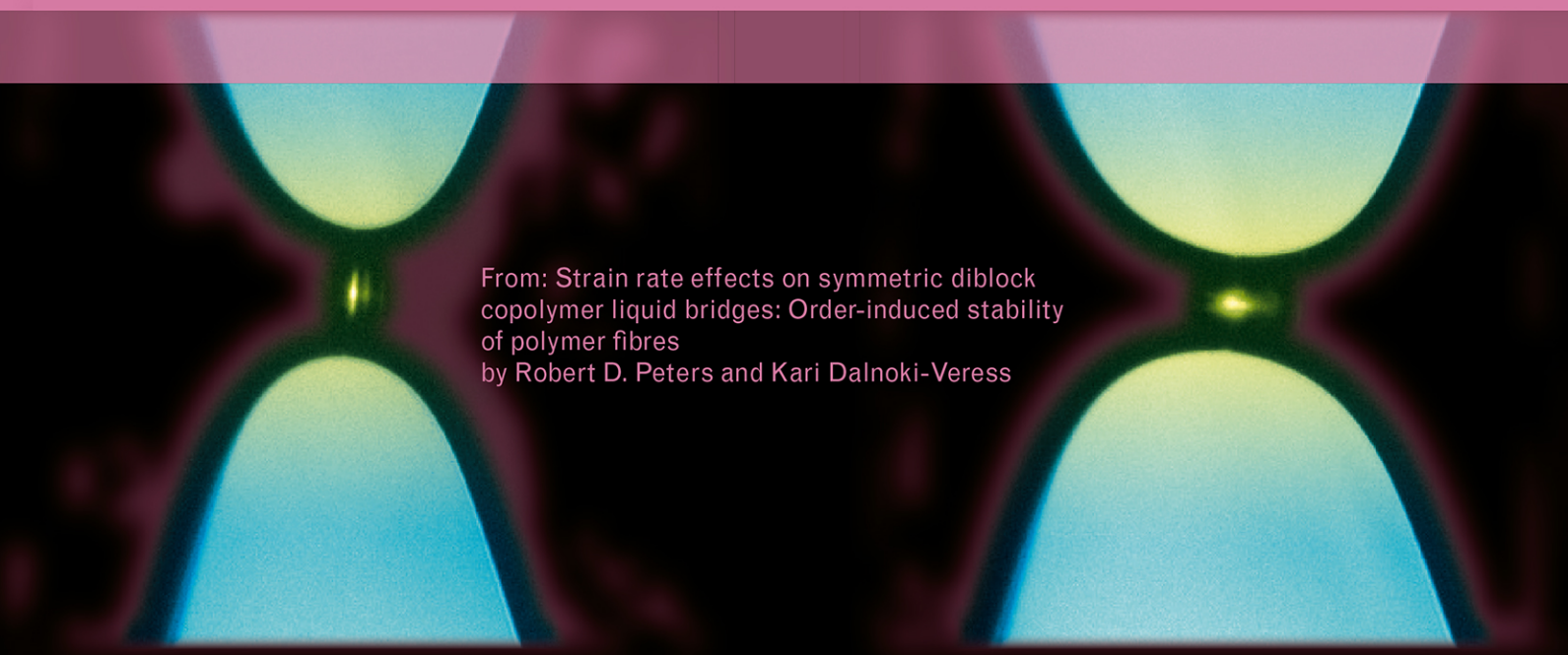

From: Strain rate effects on symmetric diblock copolymer liquid bridges: Order-induced stability of polymer fibres
by Robert D. Peters and Kari Dalnoki-Veress

edp sciences

Società Italiana di Fisica

Springer

Eur. Phys. J. E (2014) **37**: 100
DOI 10.1140/epje/i2014-14100-8

THE EUROPEAN PHYSICAL JOURNAL E

Regular Article

Strain rate effects on symmetric diblock copolymer liquid bridges: Order-induced stability of polymer fibres

Robert D. Peters[1] and Kari Dalnoki-Veress[1,2,a]

[1] Department of Physics & Astronomy and the Brockhouse Institute for Materials Research, McMaster University, Hamilton, Canada
[2] Laboratoire de Physico-Chimie Théorique, UMR CNRS 7083 Gulliver, ESPCI ParisTech, PSL Research University, Paris, France

Received 7 July 2014 and Received in final form 23 September 2014
Published online: 29 October 2014 –

Abstract. Optical microscopy is used to study the effect of lamellar order on the evolution of polymer-melt bridges. Measurements are performed on symmetric diblock copolymers and linear homopolymers in the melt state. Diblock copolymer bridges measured in the disordered phase are shown to exhibit the same strain rate response as their homopolymer counterparts: shear thinning at low strain rates and shear thickening at high strain rates. However, when measured in the ordered phase, copolymer-melt bridges demonstrate an increased effective viscosity due to the lamellar order and a shear thinning response over the entire range of strain rates probed. The increased viscosity demonstrates an enhanced stability in lamellae forming diblock liquid bridges, presumed to be caused by the isotropic orientational order of lamellar domains that provide energy barriers to flow within the bridge. The shear thinning can be understood as an alignment of lamellae along the axis of the bridge due to flow, facilitating unimpeded diffusion of polymer out of the liquid bridge along lamellar boundaries.

1 Introduction

The breakup of a long cylindrical Newtonian liquid jet into individual droplets is explained by the Plateau-Rayleigh instability. A common example of this phenomenon is the breakup of a thin stream of water from a kitchen faucet into droplets [1]. Though the water exits the faucet as a cylindrical jet, the surface is unstable to perturbations of wavelength greater than the circumference of the jet. The free energy of the thin stream is reduced via a sinusoidal perturbation that grows continuously until the jet is separated into individual droplets. Understanding the breakup of liquid jets allows us to understand many natural systems [1], however it is also vital for understanding and improving various industrial and research applications such as electrospinning [2], inkjet printing [3], and diesel engines [4], to name a few.

The breakup of a cylindrical liquid element may also be observed in the case of an unstable liquid bridge. When a droplet of fluid spanning two solid substrates is separated, for example saliva between your fingers, an axi-symmetric liquid bridge joins the two reservoirs. For small separation distances the outer curvature of the liquid bridge dominates and will induce an attractive capillary force which pulls the substrates back together [5]. However, if the separation distance is large enough then the liquid bridge is unstable as the inner curvature dominates and surface tension causes fluid to drain from the bridge into two reservoir droplets, one on each substrate [5]. In the case of a slender liquid bridge where the bridge is nearly cylindrical at its midpoint, (*i.e.* the inner curvature is much greater than the outer curvature) the minimum diameter of the bridge, $d_{\min}$, is known to evolve as

$$d_{\min} = d_0 - 2\alpha\frac{\gamma}{\eta}t, \tag{1}$$

where η is the viscosity of the liquid, γ is the surface tension, and α is a numerical geometric prefactor [6,7]. The geometric factor α has been calculated previously by Papageorgiou to be $\alpha = 0.0709$ for a liquid bridge system [6], and verified experimentally by McKinley and Tripathi [7]. Equation (1) is quite remarkable as it illustrates how one can measure a simple observable parameter in a naturally evolving system, the minimum diameter of a thinning liquid bridge, to extract an important rheological property, the ratio of surface tension to viscosity of a fluid system γ/η. The parameter γ/η is known as the capillary velocity. In the case of a simple Newtonian liquid (η is constant) and a constant surface tension, this leads to a linear decrease in filament diameter.

Though the breakup of Newtonian liquid jets and bridges is well understood [1], when additives, such as

[a] e-mail: dalnoki@mcmaster.ca

polymers, are included in a liquid jet or bridge system, the physics of breakup may become highly non-linear due to viscoelastic effects. An area of intense research focus is the breakup of dilute polymer solutions [8–17] and polymer melts [18–22]. In bulk polymer rheology, it is known that for sufficiently high strain rates, polymer melts exhibit a shear thinning property such that

$$\frac{\eta}{\gamma} = \dot{\epsilon}^{\nu}, \tag{2}$$

where $\nu < 0$ for shear thinning and $\dot{\epsilon}$ is the strain rate applied to the bulk polymer melt. For a Newtonian liquid $\nu = 0$, while $\nu > 0$ denotes shear thickening. In the case of bulk polymer systems, shear thinning has been measured with a power law exponent as large as $\nu \sim -0.85$ [23]. However, as axially symmetric polymer systems such as liquid jets and bridges evolve toward pinch-off, regions which experience a local decrease in radius also experience a stretching of the fluid element in that region, extending the polymer chains along with it. This stretching of the polymer chains by the extensional flow creates a build up of elastic stresses resulting in an increase in effective viscosity, or a shear thickening, of the liquid [8–22]. The onset of this shear thickening has been observed in dilute polymer solutions for shear strain rates that are comparable to the inverse of the polymer relaxation time [10]. This shear thickening has been shown to increase the viscosity by orders of magnitude in dilute solutions of high molecular weight polymer [8–16]. The large elongational strain rates experienced at the midpoint of a cylindrical filament, $\dot{\epsilon}$, are the source of the shear thickening and are calculated as

$$\dot{\epsilon} = \frac{1}{l}\frac{\mathrm{d}l}{\mathrm{d}t} = -\frac{2}{d_{\min}}\frac{\mathrm{d}}{\mathrm{d}t}\left(d_{\min}\right), \tag{3}$$

where l is the length of the cylindrical fluid element which is stretched upon liquid bridge thinning [11]. This localized shear thickening in regions near pinch-off leads to a variety of interesting viscoelastic effects in the breakup of both liquid bridge [13,14] and liquid jet [24] homopolymer systems.

Though extensive research has been performed on the breakup of jets and bridges both for homopolymer solutions and melts, very little has been reported on the effect of diblock copolymer architecture on the dynamics in these axially symmetric systems. Diblock copolymers consist of two chemically distinct homopolymer chains that are covalently bonded together. In the liquid state, the incompatibility between the two polymer blocks can favour phase separation at temperatures that are sufficiently low. Due to the connectivity of the two blocks, macroscale phase separation is not possible, thus diblock copolymer molecules are known to self-assemble into unique microstructures which depend on the relative lengths of the two polymer chains [25,26]. A symmetric diblock, where both blocks take up a similar volume, will microphase separate into a lamellar morphology. The lamellar thickness, L_0, is dependent on the molecular weight of the diblock and determined by the balance of both entropic and enthalpic energy terms [25]. However, as temperature is increased, the lamellar order can be destroyed as entropy becomes dominant, and the system favours mixing. The order disorder transition temperature, T_{ODT}, is determined by the relative incompatibility of the two blocks and the length of the copolymer chain [25].

A number of experimental studies have shown that diblock copolymer order has a significant effect on the rheological properties in the melt state (for example [25, 27, 28]). In particular, diblock copolymers in the disordered state can exhibit properties similar to Newtonian liquids [25]. However, in the ordered state the lamellar morphology of symmetric diblock copolymer restricts flow depending on strains and strain rates [25,28]. Here we investigate the effect of strain rate dependent rheological properties on the thinning dynamics of symmetric diblock copolymer-melt bridges.

Table 1. Polymers used in this study. M_n is the number averaged molecular weight and PI is the polydispersity index.

Polymer	M_n (kg/mol)	PI
PS	8.0	1.10
PS	16.0	1.03
P2VP	15.5	1.04
PS-b-P2VP	8.2-b-8.3	1.09
PS-b-PMMA	25-b-26	1.09

2 Experiment

2.1 Sample preparation

All measurements were performed with low polydispersity symmetric diblock copolymer and homopolymer purchased from Polymer Source Inc. (Dorval, Quebec). The homopolymers used were polystyrene (PS) and poly(2-vinylpyridine) (P2VP), while the diblocks were poly(styrene-b-2-vinylpyridine) (PS-b-P2VP) and poly(styrene-b-methyl methacrylate) (PS-b-PMMA), see table 1 for details. All polymers were dissolved in toluene to form concentrated solutions with $\sim$ 25–40% polymer by weight.

A schematic of our experimental setup is shown in fig. 1. One polymer droplet is deposited on a glass substrate that is mounted perpendicular to a freshly cleaved Si wafer (University Wafer, USA). A second droplet of the same polymer is deposited on a glass substrate that is attached to a stiff micropipette. The micropipette is affixed to a multi-axis translation stage that allows us to manoeuvre the polymer droplets in and out of contact. The entire experimental setup is then placed on a modified optical microscope hot stage (Linkam Scientific THMS 600, United Kingdom) capable of elevating the temperature, T, of the polymer above the glass transition and into the melt state. To ensure consistent temperature regulation, the experimentation volume is enclosed within a metal ring and capped with a sapphire window. The metal ring is in intimate contact with the heating block of the hot stage, and

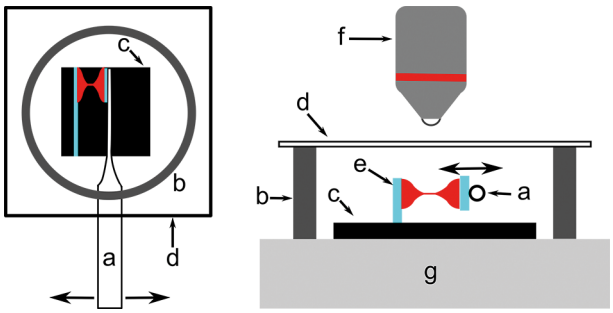

Fig. 1. Schematic of experimental setup from top view (left) and side view (right). The labels shown correspond to the different components of the setup: a) pipette, b) metal ring, c) Si wafer, d) sapphire window, e) glass substrate, f) microscope objective, g) hot stage. The pipette can be translated as indicated by the arrows in order to bring the two droplets together and prepare the liquid bridge.

the sapphire window is in contact with the metal ring. The conductive contacts and high thermal conductivity of sapphire all ensure that the temperature is well known and well controlled. All polymer droplets are annealed $\sim 50\,^{\circ}\mathrm{C}$ above the glass transition temperature for sufficient time ($\sim$ 30 min) to remove all toluene from the system and allow the droplets to relax to equilibrium spherical caps before measurements are performed.

A measurement is executed by bringing two polymer droplets into contact, causing them to coalesce (see fig. 1). The droplets are then separated quickly to a fixed distance, forming a liquid bridge that is unstable. The evolution of the polymer bridge is then monitored on an optical microscope in reflection mode (Olympus BX51, Canada). The silicon wafer provides a highly reflective background, creating high contrast between the polymer bridge and its surroundings, facilitating image analysis of the liquid bridge profile.

2.2 Time-temperature superposition

Measurements are performed over a wide range of temperatures in order to observe a broad range of dynamics. It is important to note that for all polymers used in this study, surface tension is known to vary by less than 10% over the temperature ranges used in these experiments [29], and is not dependent on the shear strain rates. However, as will be shown below, the viscosity changes by orders of magnitude. Thus, we ignore the small changes in surface tension and focus instead on the temperature and strain rate effects on viscosity which play the dominant role in dynamics. As the temperature response of the viscosity in polymeric systems is well understood, we use the Williams-Landel-Ferry (WLF) equation to perform time-temperature superposition such that all experimental time scales are shifted to those of a reference temperature [30]. The WLF equation allows us to calculate shift factors, $a_{_T}$, for specific temperatures, T, based on the equation

$$\log\left(a_{_T}\right) = -\frac{-C_1(T-T_0)}{C_2+(T-T_0)}\,, \tag{4}$$

where C_1 and C_2, are empirical constants, and T_0 is the reference temperature chosen to construct the compliance master curve in bulk rheology measurements. All time coordinates for experiments performed at different temperatures, T_1 and T_2 may be equated through the relation

$$t_1 = \left(\frac{a_{_{T_1}}}{a_{_{T_2}}}\right) t_2, \tag{5}$$

where t_1 and t_2 are the timescales of the experiments performed at temperatures T_1 and T_2, respectively [30]. Using eqs. (4) and (5), we can form master curves for experiments performed at a variety of temperatures on the same material. All measurements made above 180 °C were made under N_2 atmosphere to prevent degradation.

3 Results and discussions

In sect. 3.1 we discuss the simplest case of the 8 kg/mol PS homopolymer —this simple canonical system will serve as a reference for the measurements on diblock copolymers. In sect. 3.2 we discuss the diblock copolymers. First a PS-b-P2VP with a total molecular weight of 16 kg/mol which has an experimentally accessible T_{ODT}. As will be seen, the lamellar order resulting from the microphase separation in symmetric diblock copolymer melts has a significant effect on the breakup dynamics of the bridges. We will then compare the 16 kg/mol PS-b-P2VP to both PS and P2VP homopolymer, both with the same molecular weight as the diblock. Ensuring that the PS-b-P2VP, PS, and P2VP all have similar molecular weights facilitates a fair comparison of the dynamics. The second diblock studied is PS-b-PMMA diblock which is strongly segregated and serves as a comparison to the PS-b-P2VP to investigate the general features of diblock fibres.

3.1 Homopolymer bridges

To facilitate comparison to the more complex case of diblock copolymers, we performed experiments on a linear, 8 kg/mol PS homopolymer, which is well below the entanglement molecular weight. The evolution of a typical homopolymer bridge is shown in fig. 2. Initially, after the droplets are separated, there is a significant outer curvature in the bridge (fig. 2a). After a short time, the liquid bridge forms an approximately cylindrical fiber, with negligible outer curvature at the midpoint (fig. 2b) and this liquid cylinder decreases in diameter until its eventual pinch-off (fig. 2c-d). Due to the high contrast between the polymer and the highly reflective Si wafer background, the diameter of the bridge is easily measured as a function of time, resulting in a typical plot shown in fig. 3. In that plot it can be seen that in the early stages, after initial droplet separation, the dynamics are highly nonlinear ($t \lesssim 0.5$ min, see also image in fig. 2a); however, after the bridge evolves to a cylindrical geometry we can use eq. (1) to obtain the evolution of viscosity in the system.

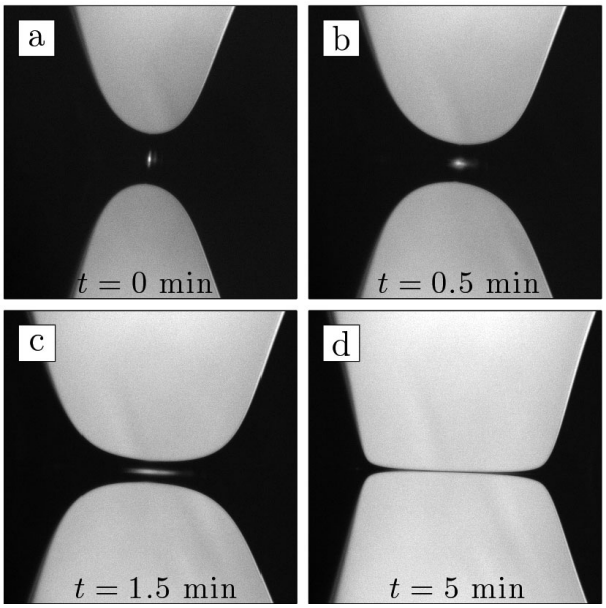

Fig. 2. Optical microscopy images of stages of liquid bridge evolution for 8 kg/mol PS homopolymer melt at 130 °C. All images are 500 μm wide.

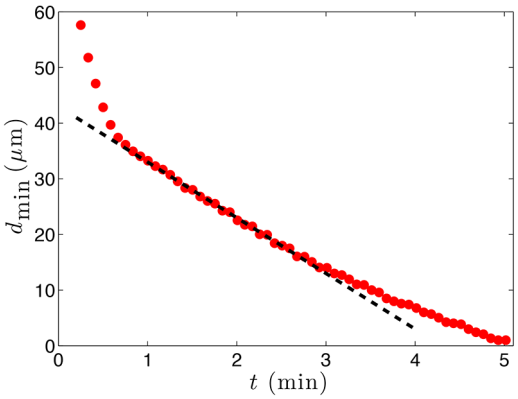

Fig. 3. Typical measurement of minimum diameter ($d_{\min}$) as a function of time for homopolymer, taken for 8 kg/mol PS bridge at 130 °C. The dashed line identifies the approximately constant viscosity regime after the cylindrical bridge is formed. Deviations from the simple Newtonian fluid can be identified by the decrease in the slope at late times, which corresponds to an increase in viscosity.

In this measurement, when the nearly cylindrical geometry is reached ($t \sim 0.5$ minutes), $d_{\min}$ decreases linearly with time indicating a constant viscosity. However, as the diameter of the bridge decreases, the bridge evolution deviates from this linearity. Clearly the bridge begins to thin more slowly. Since $1/\eta$ is proportional to the slope of the plot in fig. 3 (see eq. (1)), the slowing down indicates an increasing viscosity for small bridge diameters.

Since an instantaneous η/γ and $\dot{\epsilon}$ can be calculated from $d_{\min}(t)$ using eqs. (1) and (3), respectively, we can monitor the effect of strain rate on the viscosity of our system. All results presented hereafter for η/γ as a function of $\dot{\epsilon}$ are calculated from the average of at least 4 separate

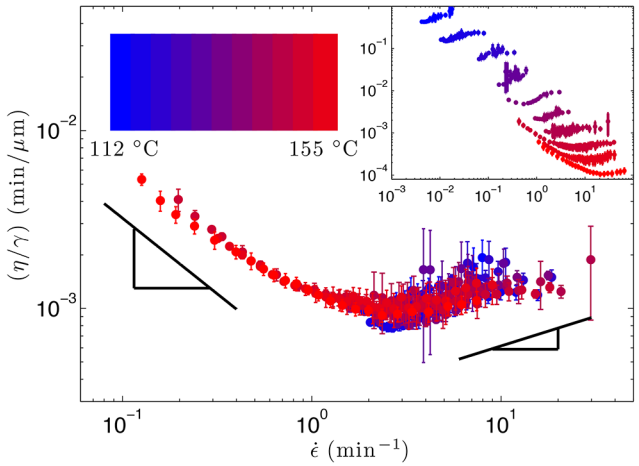

Fig. 4. Measurement of the ratio of viscosity to surface tension as a function of strain rate at the midpoint of the liquid bridge for temperatures of 112 °C to 155 °C for PS with 8 kg/mol. The data has been shifted using the WLF equation as described in the text. The two power law slopes represent guides to the eye for the shear thinning and shear thickening representing power laws of $\nu = -0.85$ and $\nu = 1/3$, respectively, in correspondence with eq. (3). The inset demonstrates the unshifted data for each temperature.

liquid bridge breakup experiments at each temperature. Measurements on 8 kg/mol PS were performed over a temperature range of 112 °C to 155 °C, allowing us to probe a wide range of different strain rates and polymer viscosities. The viscosity changes by orders of magnitude and is known to be impacted by shear flows in both bulk and liquid bridge systems [22,23]. By applying time-temperature superposition using eqs. (4) and (5), we shift all measurements to a reference temperature of 140 °C obtaining a master curve of all data. We use WLF shift parameters for PS of $C_1 = 15$ °C, $C_2 = 60$ °C, and $T_0 = 98$ °C, taken from ref. [31].

In fig. 4 is shown the data for η/γ and $\dot{\epsilon}$, both without time-temperature superposition (inset) and the superposed data for the 8 kg/mol PS. From the inset it is clear that over 4 orders of magnitude in viscosity and strain rate are observed for the different temperatures. The temperature shifted data (main plot) shown in fig. 4 illustrates an excellent collapse of all the data. A transition between two regimes for the viscosity at the midpoint of the homopolymer bridge as a function of strain rate is observed. At low strain rates, the polymer bridge decreases in viscosity as a function of strain rate, indicative of a shear thinning fluid. This shear thinning approaches a power law (see eq. (2)) with an exponent of $\nu \sim -0.85$, indicating bulk shear response in accordance with previous measurements [23]. However, at higher strain rates there is a transition to a shear thickening regime, where the viscosity increases as a function of strain rate within the bridge. This is in response to the high elongational flow experienced in the liquid bridge geometry extending polymer chains, thereby increasing the effective viscosity of the homopolymer melt [10]. The shear thickening effect is

not as drastic as in previous experiments [11–16], where viscosity was observed to increase by orders of magnitude, for 2 main reasons. Firstly, our strain rates are lower than in these previous experiments. Secondly, previous experiments were performed primarily on polymer solutions and homopolymers of much larger molecular weight, increasing the relaxation time of the polymer and creating a greater build up of elastic stresses due to extensional flows.

3.2 Symmetric diblock copolymer bridges

Having understood the dynamics in the simple homopolymer system, we now focus on the effect of lamellar ordering of symmetric diblocks on the dynamics of copolymer bridges. We use PS-b-P2VP which has an experimentally accessible bulk T_{ODT} of $\sim 160\,^{\circ}\mathrm{C}$ [32]. Simply by changing temperature we can treat this system as a simple homogenous polymer fluid, like the PS homopolymer case discussed above, or as a complex fluid with ordered lamellae. Furthermore, PS-b-P2VP was chosen as both PS and P2VP are similar in terms of chemical composition and have similar rheological properties [33]. As before, we measure the PS-b-P2VP at varying temperatures from $150\,^{\circ}\mathrm{C}$ to $180\,^{\circ}\mathrm{C}$, thereby capturing the dynamics above and below T_{ODT}. Optical images of evolution and the corresponding typical measurements of $d_{\mathrm{min}}(t)$ are shown in fig. 5 for the disordered state at $175\,^{\circ}\mathrm{C}$ (fig. 5a) and ordered state at $155\,^{\circ}\mathrm{C}$ (fig. 5b). The left-right asymmetry seen in the optical images reflects slightly different geometries for the left droplet and right droplet prior to coalescence. This asymmetry is not a concern since the system is locally symmetric at the minimum diameter, from where the measurement $d_{\mathrm{min}}(t)$ is obtained. Though it is difficult to compare measurements made at the two temperatures shown in fig. 5, the difference in evolution of $d_{\mathrm{min}}(t)$ is marked. While the disordered diblock copolymer exhibits dynamics similar to what we observed for the homopolymer case (fairly constant viscosity), the ordered lamellar diblock bridge evolves differently, thinning out much faster as the liquid bridge gets thinner and strain rates increase at $t \gtrsim 25\,\mathrm{min}$.

Since diblock copolymer melts are a complex fluid with nanostructure, it is difficult to define a viscosity or surface tension[1] for the system. However, since the evolution of diblock bridges is cylindrical at the midpoint for the late stages of breakup, we can calculate an effective viscosity, $(\gamma/\eta)_{\mathrm{eff}}$, and strain rate using eqs. (1) and (3). The calculation of an effective viscosity in diblock copolymer systems has been performed in the past using bulk rheological techniques [25]. In fig. 6 we show the results of $(\eta/\gamma)_{\mathrm{eff}}$ as a function of $\dot{\epsilon}$. The raw unshifted data is shown in the inset and, as in the homopolymer case, an increase in temperature is accompanied by orders of magnitude decreases in viscosity. However, the shear response of the low temperature lamellar ordered diblock melt is quite different from

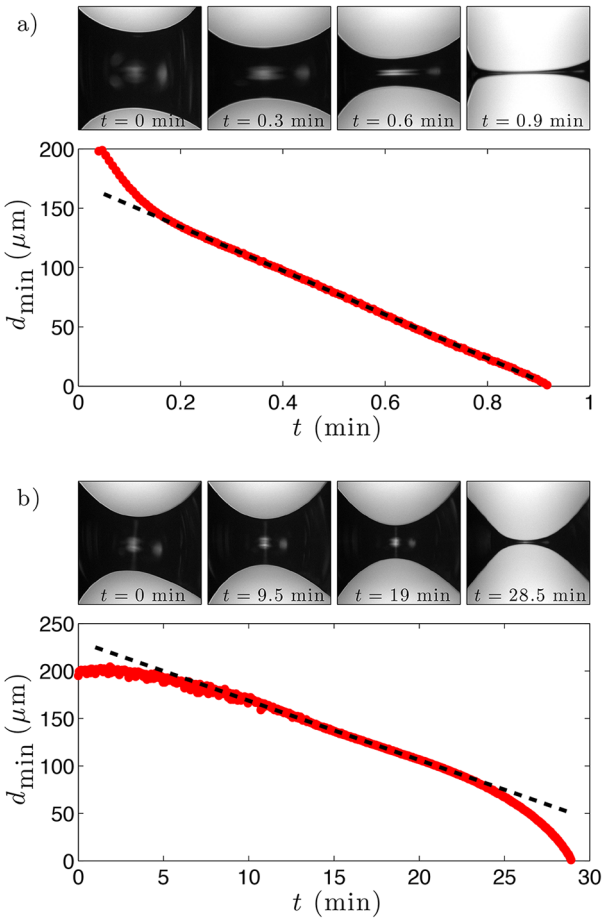

Fig. 5. Typical measurement of the minimum diameter as a function of time for the bridge evolution of PS-b-P2VP in the disordered (top) and ordered (bottom) state at $175\,^{\circ}\mathrm{C}$ and $155\,^{\circ}\mathrm{C}$, respectively. The dashed lines identify the constant viscosity regimes. The optical microscopy images (times indicated) are representative of the breakup of the diblock bridges. The images are $500\,\mu\mathrm{m}$ wide.

the high temperature disordered melt, exhibiting solely shear thinning response during the liquid bridge evolution. This shear thinning response is entirely consistent with the increasing negative slope of fig. 5b).

In addition to experiments on lamellar forming 16.5 kg/mol PS-b-P2VP, we also performed measurements on 16 kg/mol homopolymer PS and 16 kg/mol homopolymer P2VP melt bridges to facilitate comparison. Since both PS and P2VP exhibit extremely similar rheological properties (both in previous measurements [33] as well as the liquid bridge evolution experiments performed with our experimental setup), we performed time-temperature superposition of all PS, P2VP and PS-b-P2VP with the same WLF shift parameters as before using eqs. (4) and (5). In the main plot of fig. 6 is shown the effective ratio of viscosity to surface tension as a function of strain rate for all three polymer melts superposed to a temperature of $140\,^{\circ}\mathrm{C}$. As expected, the homopolymer PS and P2VP data collapse to similar viscosities and strain rate responses. Just as the 8 kg/mol PS of fig. 4, there is an initial shear

[1] Again, we stress that though the surface tension may differ, the changes are at the 10% level while the effective viscosity changes by orders of magnitude.

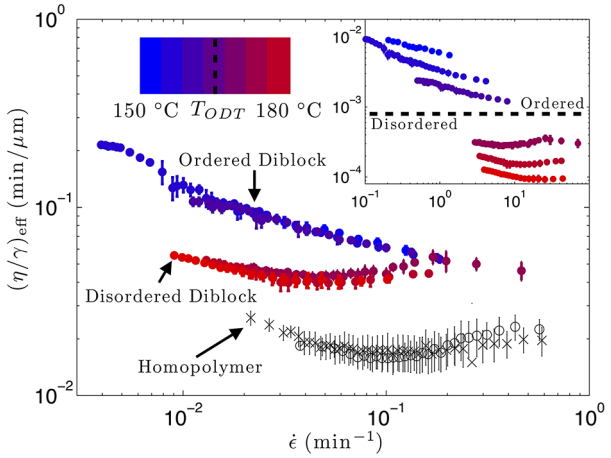

Fig. 6. Measurement of the ratio of viscosity to surface tension as a function of strain rate during bridge evolution for 16 kg/mol PS-b-P2VP (filled circles), 16 kg/mol linear PS (open circles), and 16 kg/mol linear P2VP (crosses). All the data in the main plot has been superposed using the PS WLF parameters. The inset shows the same PS-b-P2VP data unshifted by time-temperature superposition. The horizontal dashed line indicates the separation between measurements made in the ordered and disordered states.

thinning regime followed by a shear thickening with increasing shear strain rate. However, when we perform time-temperature superposition on the diblock copolymer data, we obtain a remarkable collapse of the data to *two* markedly different master curves corresponding to the ordered and disordered diblock phases.

All experiments performed in the disordered phase, collapse to a single curve that exhibits a similar shear response to that of the homopolymer PS and P2VP systems, whereby there is a shear thinning effect at low strain rates, and a shear thickening effect at high strain rates. At these high temperatures, there is no order and the homogeneous diblock system is rheologically equivalent to a homopolymer. This result is in agreement with measurements performed on bulk disordered diblock copolymers, where similar rheological properties to simple homopolymers were observed [25, 28]. One interesting and surprising result for disordered diblock bridges is that though they have similar shear responses, they exhibit increased effective viscosity in comparison to the experiments on homopolymers of each block, though all three molecules were chosen to have very similar molecular weight. We speculate that this may be caused by an increased energy cost of flowing unlike blocks past each other in the melt, even in the disordered case where the diblock copolymers are a homogeneous mixture.

The measurements made in the ordered lamellar phase, below $T_{\rm ODT}$, collapse to a distinct second curve. The measurements on ordered diblock copolymer demonstrate an elevated effective viscosity at low shears in comparison to measurements made in the disordered state, indicating an enhanced stability of ordered diblock-melt bridges. Additionally, the strain rate response is shear thinning throughout the entire measurement, recombining with the disordered data only at the largest strain rates just before bridge breakup. Since all measurements were performed on the same diblock copolymer droplets, *the difference in dynamics is attributed solely to the effect of order on the flow* in symmetric diblock bridges.

In order to understand the results for the lamellar ordered diblock, we first revisit the length scales in the system. The symmetric diblock copolymer orders with a repeating bilayer thickness on the $\sim$ 10 nm length scale, $L_0 \approx 13.5$ nm, whereas the polymer bridge diameter is initially 10s to 100s of microns in diameter. This represents a difference of 10^3–10^4 in length scale between the lamellae and the entire system, indicating that we may treat our liquid bridges as an unconfined, bulk system with regard to the diblock ordering. In bulk symmetric diblock copolymer systems ordered under low shear or no shear, the orientation of lamellar domains is isotropic [25]. Thus, within our bridge there are lamellae oriented in many different directions. Though polymer may flow along the boundary of a lamella continuously, there is an energy barrier to hopping from one lamellar layer to another [34], or hopping across defects between lamellae of different orientations [35]. The energy barrier to layer hopping or motion across a defect is induced by the energy cost of moving a polymer block through a region of unlike polymer. In the case of our ordered symmetric diblock-melt bridges, due to the isotropic orientations of the lamellae, there are countless energy barriers that must be overcome in flowing polymer from the centre of the bridge to the reservoir droplets. These energy barriers impede flow and consequently increase the effective viscosity of the system and the inherent stability of the polymer bridge.

We now turn to the shear thinning that is observed over the entire range of shear strain rate explored for the ordered diblocks. As the ordered diblock bridge thins in diameter, strain rates increase and as is evident from fig. 6, the effective viscosity decreases. It is known that in the case of oscillatory shear measurements made on bulk symmetric diblock copolymer melts in the ordered phase, the lamellar domains may become aligned with shear forces dependent on annealing history as well as the amplitude and frequency of shear [36]. Additionally, the application of sufficiently large shear stress is known to align lamellae, cylinders and spheres in block copolymer thin films [37,38]. The process is believed to occur through the destruction of ordered domains not oriented parallel to the shear stress, and the subsequent reformation of ordered structures in alignment with applied shear [39, 40]. Since we measure shear thinning in our measurements on ordered diblock-melt bridges, we suggest that the strain rates within the bridge are in the regime where lamellae are forced to align such that the normal vector to the lamellae are directed perpendicular to the flow. This orientation would allow copolymer to travel more efficiently along the lamellar boundaries, flowing into the reservoir droplets without having to hop between lamellae or across as many defects. As the strain rates increase, the lamellae become increasingly more aligned and the effective viscosity correspondingly decreases.

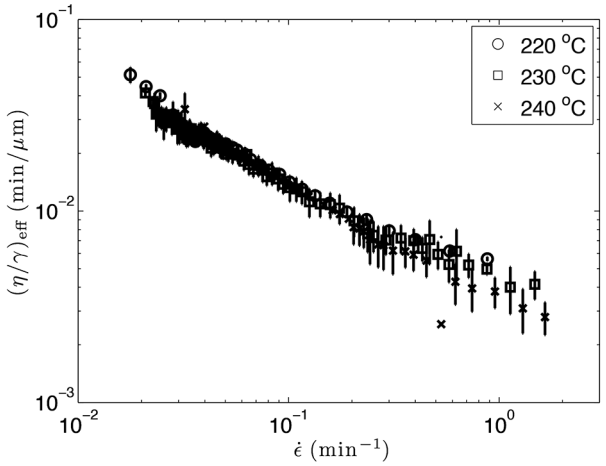

Fig. 7. Measurements of effective viscosity divided by surface tension as a function of strain rate for a 51 kg/mol PS-b-PMMA symmetric copolymer. Measurements are not shifted using time-temperature superposition.

In addition to this shear thinning effect, it is evident from fig. 6 that measurements made both above and below T_{ODT} converge at high strain rates to the same effective viscosity. There are two possible explanations for this convergence; the disordered phase is ordering under shear *or* the ordered phase is disordering. In bulk systems, oscillatory shear has been shown to increase the T_{ODT} for lamellar forming diblocks, and the domains created under these conditions are aligned such that flow is possible along the lamellar boundaries [41,42]. Therefore, it seems likely that under the strain rates experienced in our measurements, the disordered diblock is ordering lamellae at high strain rates such that flow is less impeded and dynamics are identical to measurements performed below bulk T_{ODT}. Indeed this suggestion is further evidenced by the fact that the disordered diblock, rather than continuing along the trend of shear tickening with increasing $\dot{\epsilon}$ actually follows perfectly the extrapolated shear thinning trend of the ordered diblock.

Bridge evolution measurements were also performed on a 51 kg/mol PS-b-PMMA symmetric diblock copolymer which has an experimentally unaccessible T_{ODT}, and thus contains more strongly segregated lamellae than its PS-b-P2VP counterpart [43]. Polymer-melt bridge evolution was investigated at 220, 230 and 240 °C for the PS-b-PMMA melt in a N_2 atmosphere. In fig. 7 we plot the effective viscosity divided by surface tension as a function of strain rate for the PS-b-PMMA copolymer without performing any time-temperature shifts. It is clear that for this highly ordered polymer melt, a shear thinning effect is once again observed due to the shear alignment of lamellae along the direction of flow within the bridge. However, it is interesting to note that in the case of this highly ordered symmetric diblock, the effect of temperature seems to be negligible since the dynamics at all 3 temperatures seem to overlap. As the PS-b-PMMA system is more strongly segregated, there is a much larger energy penalty for layer hopping or moving across a defect than for the weakly ordered PS-b-P2VP melt. We speculate that the dynamics are dominated by the shear alignment of the lamellae, rather than the viscosity effects of the individual polymer blocks, resulting in identical dynamics for measurements at different temperatures.

An increase in effective viscosity upon lamellar ordering and a decrease in viscosity upon application of strain has been observed previously in oscillatory shear rheology experiments [25, 27, 28]. In particular, Schulz *et al.* performed measurements on a PS-P2VP diblock copolymer and observed a discontinuity in the rheological properties as a function of temperature for constant shear rates [27]. This discontinuity is consistent with a transition from the ordered to the disordered curves in fig. 6. The collapse of ordered and disordered data with only time-temperature superposition from a direct observation of bridge diameter supports previous rheological measurements of symmetric diblock copolymer. As well, the additional complexity of the elongational flows within the axisymmetric liquid bridges provides a useful method for studying complex macromolecular fluids where molecule extension or alignment may play a key role in the resultant dynamics.

4 Conclusions

Using optical microscopy we have investigated the effect of the lamellar order in symmetric diblock copolymer melts on the dynamics of unstable polymer-melt bridges. In the disordered phase, symmetric diblock copolymer melts were observed to exhibit similar dynamics to their homopolymer counterparts: at low strain rates, a shear thinning response due to bulk shear effects, followed by a shear thickening response due to polymer extension at high strain rates. Though qualitatively similar to the homopolymers in response to strain rate, the symmetric diblock copolymer in the disordered state was measured to have higher effective viscosity than the homopolymers. In the ordered phase, symmetric diblock copolymers were observed to be markedly different from disordered. The ordered system was more stable, with a higher effective viscosities in comparison to the disordered phase. This enhanced stability may be attributed to the energy barriers to flow induced by the isotropic orientation of lamellae. As strain rates increased, a shear thinning response was measured consistent with an alignment of lamellae which facilitates flow of polymers from the bridge into the adjacent droplets. In the case of the strongly segregated lamellar forming diblock, PS-b-PMMA, the effect of temperature was negligible in comparison to the shear thinning effect in the liquid bridge evolution, exhibiting identical dynamics over a 20 °C temperature range. The ability of diblock copolymers to prevent breakup and enhance the stability of liquid fibres may be useful for the production of textiles or in the creation of electrospun fibres.

Financial Support for this work was provided by National Sciences and Engineering Research Council (NSERC). The authors thank Mark Matsen and An-Chang Shi for helpful discussions.

References

1. J. Eggers, E. Villermaux, Rep. Prog. Phys. **71**, 036601 (2008).
2. D.H. Reneker, A.L. Yarin, Polymer **49**, 2387 (2008).
3. B.J. de Gans, P.C. Duineveld, U.S. Schubert, Adv. Mater. **16**, 203 (2004).
4. C. Arcoumanis, J.H. Whitelaw, J. Mech. Engin. Sci. **201**, 57 (1987).
5. L.E. Johns, R. Narayanan, *Interfacial Instability* (Springer, New York, 2002).
6. D.T. Papageorgiou, Phys. Fluids **7**, 1529 (1995).
7. G.H. McKinley, A. Tripathi, J. Rheol. **44**, 653 (2000).
8. V.M. Entov, E.J. Hinch, J. Non-Newtonian Fluid Mech. **72**, 31 (1997).
9. M.I. Kolte, P. Szabo, J. Rheol. **43**, 609 (1999).
10. Y. Amarouchene, D. Bonn, J. Meunier, H. Kellay, Phys. Rev. Lett. **86**, 3558 (2001).
11. S.L. Anna, G.H. McKinley, J. Rheol. **45**, 115 (2001).
12. C. Clasen, J. Eggers, M.A. Fontelos, J. Li, G.H. McKinley, J. Fluid Mech. **556**, 283 (2006).
13. R. Sattler, C. Wagner, J. Eggers, Phys. Rev. Lett. **100**, 164502 (2008).
14. P.P. Bhat, S. Appathurai, H.M.T., M. Pasquali, G.H. McKinley, O.A. Basaran, Nat. Phys. **6**, 625 (2010).
15. R. Sattler, S. Gier, J. Eggers, C. Wagner, Phys. Fluids **24**, 023101 (2012).
16. A.V. Bazilevskii, Fluid Dyn. **48**, 97 (2013).
17. J. Eggers, Phys. Fluids **26**, 033106 (2014).
18. A. Bach, K. Almdal, H.K. Rasmussen, O. Hassager, Macromolecules **36**, 5174 (2003).
19. M.H. Wagner, S. Kheirandish, O. Hassager, J. Rheol. **49**, 1317 (2005).
20. Y. Wang, P. Boukany, S.Q. Wang, X. Wang, Phys. Rev. Lett. **99**, 237801 (2007).
21. H.K. Rasmussen, K. Yu, Phys. Rev. Lett. **107**, 126001 (2011).
22. M.H. Wagner, V.H. Rolon-Garrido, J. Rheol. **56**, 1279 (2012).
23. W.W. Graessley, Adv. Polym. Sci. **16**, 1 (1974).
24. C. Clasen, J. Bico, V. Entov, G.H. McKinley, J. Fluid Mech. **636**, 5 (2009).
25. G.H. Fredrickson, F.S. Bates, Annu. Rev. Mater. Sci. **26**, 501 (1996).
26. M.J. Fasolka, A.M. Mayes, Annu. Rev. Mater. Res. **31**, 323 (2001).
27. M. Schulz, A. Khandpur, F.S. Bates, K. Almdal, K. Mortensen, D. Hajduk, S. Gruner, Macromolecules **29**, 2857 (1996).
28. J.H. Rosedale, F.S. Bates, Macromolecules **23**, 2329 (1990).
29. S. Wu, J. Phys. Chem. **74**, 632 (1970).
30. M.L. Williams, R.F. Landel, J.D. Ferry, J. Am. Chem. Soc. **77**, 3701 (1955).
31. J.E. Mark (Editor) *Physical Properties of Polymers Handbook* (AIP Press, New York, 1996).
32. A.B. Croll, A.C. Shi, K. Dalnoki-Veress, Phys. Rev. E **80**, 051803 (2009).
33. Y. Takahashi, N. Ochiai, Y. Matsushita, I. Noda, Polym. J. **28**, 1065 (1996).
34. A.B. Croll, M.W. Matsen, A.C. Shi, K. Dalnoki-Veress, Eur. Phys. J. E **27**, 407 (2008).
35. D. Duque, K. Katsov, M. Schick, J. Chem. Phys. **117**, 10315 (2002).
36. V.K. Gupta, R. Krishnamoorti, Z.R. Chen, J.A. Kornfield, S.D. Smith, M.M. Satkowski, J.T. Grothaus, Macromolecules **29**, 875 (1996).
37. A.P. Marencic, D.H. Adamson, P.M. Chaikin, R.A. Register, Phys. Rev. E **81**, 011503 (2010).
38. G. Singh, K.G. Yager, B. Berry, H.C. Kim, A. Karim, ACS Nano **6**, 10335 (2012).
39. S. Pujari, M.A. Keaton, P.M. Chaikin, R.A. Register, Soft Matter **8**, 5858 (2012).
40. B.L. Peters, A. Ramirez-Hernandez, D.Q. Pike, M. Muller, Macromolecules **45**, 8109 (2012).
41. K.A. Koppi, M. Tirrell, F.S. Bates, Phys. Rev. Lett. **70**, 1449 (1993).
42. L. You, Y.D. He, Y. Zhao, Z.Y. Lu, J. Chem. Phys. **129**, 204901 (2008).
43. T.P. Russell, R.P. Hjelm, P.A. Seeger, Macromolecules **23**, 890 (1990).